Oscillator strength reduction induced by external electric fields in self-assembled quantum dots and rings

Benito Alén,[1,2,*] José Bosch,[1] Daniel Granados,[2] Juan Martínez-Pastor,[1] Jorge M. García,[2] and Luisa González[2]
[1]Instituto de Ciencia de los Materiales, Universidad de Valencia, P.O. Box 2085, 46071 Valencia, Spain
[2]Instituto de Microelectrónica de Madrid (CNM, CSIC), Isaac Newton 8, 28760, Tres Cantos Madrid, Spain
(Received 10 July 2006; revised manuscript received 6 November 2006; published 10 January 2007)

We have carried out continuous wave and time resolved photoluminescence experiments in self-assembled In(Ga)As quantum dots and quantum rings embedded in field effect structure devices. In both kinds of nanostructures, we find a noticeable increase of the exciton radiative lifetime with the external voltage bias that must be attributed to the field-induced polarizability of the confined electron hole pair. The interplay between the exciton radiative recombination and the electronic carrier tunneling in the presence of a stationary electric field is therefore investigated and compared with a numerical calculation based on the effective mass approximation.

DOI: 10.1103/PhysRevB.75.045319 PACS number(s): 81.07.Ta, 78.67.Hc, 73.63.Kv, 73.21.La

I. INTRODUCTION

The quantum confined Stark effect (QCSE) was first studied in quantum-well (QW) structures subjected to a stationary electric field applied in the growth direction.[1–4] In the presence of the field, direct tunneling of either electrons or holes, out of the well and through the triangular potential barrier, competes with other recombination processes determining the effective lifetime of the confined carriers. Given the high quality of current growth methods, at low temperature we can neglect other nonradiative mechanisms to study the interplay between radiative recombination and carrier tunneling as a function of the applied field. In this work we will investigate such interplay in self-assembled In(Ga)As quantum dots (QDs) and quantum rings (QRs) embedded in a field effect structure device.

A well established notion about exciton dynamics in these kinds of nanostructures is that, in analogy to QWs, carrier tunneling is responsible for the photoluminescence (PL) quenching observed at moderate reverse voltages.[5] In this way, it is usual in the literature to overlook the reduction of the ground state oscillator strength resulting from the electron and hole separation induced by the QCSE. This assumption is justified at high electric fields when direct tunneling is up to two orders of magnitude faster than radiative recombination. However, in applications where the optical detection or manipulation of the QD electronic configuration is performed at low or moderate electric fields, the QCSE can be more relevant or even dominate, as demonstrated in this work.[6,7]

Simultaneous determination of the photoluminescence (PL) and photocurrent (PC) spectra of single quantum dots have been reported by several authors demonstrating, through analysis of the PC resonance linewidth, a fast decrease of the exciton lifetime for externally applied reverse electric fields $F \geqslant 85$ kV/cm.[8–10] Differential transmission experiments have been carried out at the single QD level to study the tunneling regime with improved spectral resolution.[11] However, even the most precise methods in the spectral domain are not enough yet to resolve an increase of the radiative lifetime above ~ 1 ns.[12–14] The analysis in the temporal domain is mandatory in this case, but we found that few time resolved studies of In(Ga)As quantum dots embedded in field effect devices have been reported, and in particular, little attention has been paid to the implications of the QCSE over the exciton radiative lifetime.[15–17] This study however, has been carried out in II/VI semiconductor nanocrystals and theoretically described on its basis.[18–20]

In this work, we investigate the modification of the exciton radiative lifetime induced by the QCSE in In(Ga)As nanostructures with different sizes and shapes. We carry out continuous wave and time resolved photoluminescence experiments to decouple the radiative and nonradiative (electron tunneling) contributions to the exciton lifetime. Also, the experimental decay times are compared with a numerical calculation including the three dimensional carrier confinement of excitons and the electron tunneling out of the dots through a triangular barrier.

II. SAMPLES AND EXPERIMENT

Two samples have been investigated containing self-assembled QDs or QRs embedded in the intrinsic region of nominally identical Schottky diodes. Solid source molecular beam epitaxy growth started depositing an AlAs/GaAs short period superlattice over a semi-insulating GaAs substrate. Thereafter, the back contact layer was formed by depositing 20 nm of Si-doped n^+-GaAs. The nanostructures are separated from the back contact by a 25 nm-thick GaAs spacer layer that acts as tunneling barrier for the electrons in the reverse bias state. The heterostructure was completed with an AlAs/GaAs blocking barrier and a 4 nm-thick GaAs capping layer. Finally, semitransparent Ni-Cr Schottky gates and diffused Au-Ge-Au back contacts were developed using standard photolithographic techniques.

For the aim of our study, atomic force microscopy (AFM) characterization was performed in equivalent uncapped samples. Using low growth rates, deposition of 2.5 ML of InAs at 480 °C gives rise to an inhomogeneous distribution of 5×10^{10} cm^{-2} QDs, with typical dot height values around 7 ± 3 nm and 1:3 aspect ratio. They are representative of our QD sample with a room temperature emission peak wave-

 ©2007 The American Physical Society

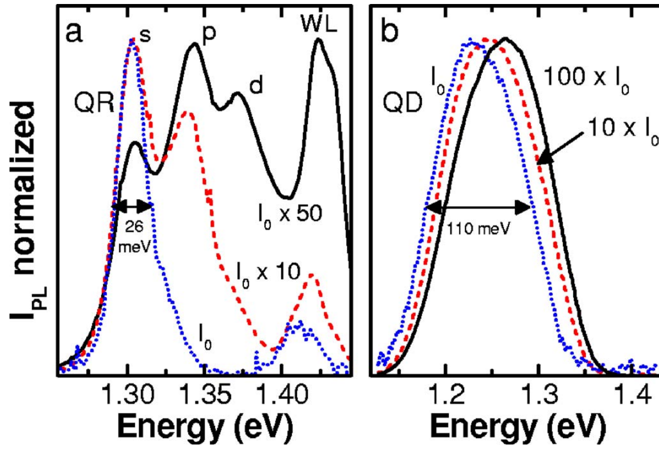

FIG. 1. (Color online) Normalized emission spectra obtained in the quantum ring (QR) and quantum dot (QD) samples increasing the excitation power density of an Argon laser at 15 K. (a) The QR sample exhibit a clear shell-filling effect characteristic of emission from excited states. (b) The evolution of the QD PL band is typical of highly inhomogeneous size distributions.

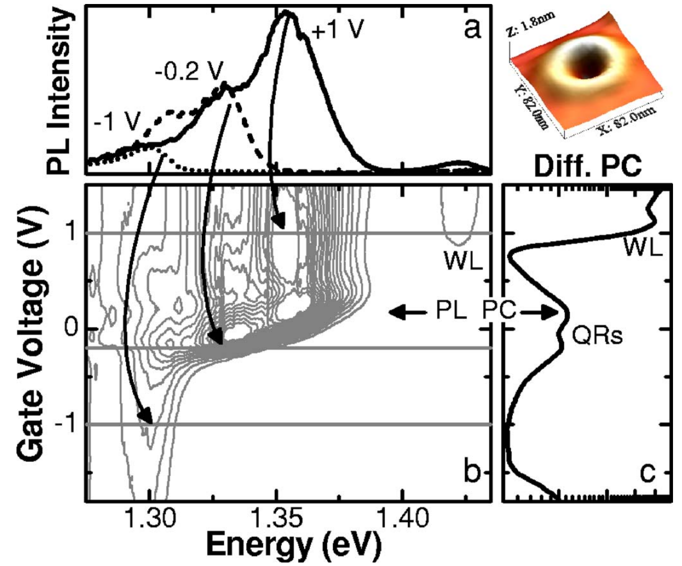

FIG. 2. (Color online) Quantum rings sample: (a) Three PL spectra are shown revealing the evolution of the emission band with applied electric field at 15 K. (b) Contour line plot of the photoluminescence covering the full voltage range. (c) Differential photocurrent spectrum obtained upon laser excitation over the GaAs band edge. Strong resonances are observed when tunneling of electrons into the bound states or into the WL is allowed. Inset: AFM image of an uncapped quantum ring.

length at 1.12 eV. The self-assembled quantum rings are obtained by partially covering with GaAs a layer containing QDs with bigger average heights ($h > 11$ nm). A detailed description of the growth procedure can be found elsewhere.[21,22] In this case, AFM images reveal rather flat ring-shaped nanostructures ($h < 4$ nm and aspect ratio $> 1:20$) whose emission wavelength is shifted to 1.26 eV at room temperature. Also, due to the different growth conditions, the areal density is one order of magnitude smaller in this case.

Time resolved photoluminescence (TRPL) spectra were measured at 15 K by using a Ti:sapphire laser emitting at 820 nm and operating with ~2 ps pulsewidth at 76 MHz of repetition rate (Coherent Mira 900D). The light collected from the sample by a low amplification objective was dispersed by an imaging 0.5 m focal length spectrograph and detected with a streak camera (Hamamatsu C5680) giving an overall time resolution of ~40 ps. Continuous wave experiments at the same temperature were performed with a standard PL setup using as excitation source either the same laser under CW operation ($\lambda = 820$ nm) or an Ar laser ($\lambda = 514$ nm). The collected light was dispersed by a 0.3 m focal length monochromator and detected with a S1-type photon counting module for the QD sample, or a back-illuminated cooled charge coupled device for the QR sample. Additionally, a programmable voltage source and a lock-in amplifier have been used to apply the desired bias and monitor the device photocurrent signal (PC).

III. CONTINUOUS WAVE CHARACTERIZATION

The PL spectra shown in Fig. 1 have been obtained at 15 K illuminating with the Ar laser focused beam a region far away from the gate contact. At low excitation power ($I_0 \sim 0.5$ kW/cm^2), the PL spectrum bandwidth reflects the QD/QR size inhomogeneity. Quantum rings are characterized by a narrow band (~26 meV broad) peaked at 1.3 eV, although minor contributions are visible at higher energies [Fig. 1(a)]. Due to the low areal density of this sample, the increase of the pumping power gives rise rapidly to the saturation of the QR's ground state. This saturation is accompanied by the appearance of two additional emission bands together with the wetting layer (WL) resonance contribution at ~1.42 eV. This is the expected behavior for a narrow size distribution of QRs in a low density sample (typically below 5×10^9 cm^{-2}) showing strong excited state radiative recombination.[23] The evolution of the PL for the QD ensemble is quite different, as observed in Fig. 1(b). The initial band at low power is centered at 1.23 eV and already ~110 meV broad. Increasing the excitation density, the emission is only slightly shifted to higher energies, the shell filling effect being much less important than in the QR sample. In this case, the broad PL band corresponds to a broad distribution of QDs with a high areal density (typically above 5×10^{10} cm^{-2}), as it has been reported in previous studies of similar intrinsic samples.[24]

Both samples have been characterized monitoring the PL and PC signal under different bias conditions. The spectra were measured as a function of the external voltage illuminating the sample at the GaAs band edge to create electron-hole pairs only in the vicinity of the nanostructures. The devices exhibit negligible dark currents and noticeable photocurrents at the voltages studied here.

Figures 2(a) and 3(a) show the PL spectra obtained at three different voltages for QRs and QDs, respectively. The full bias evolution for each sample is depicted in contour line plots underneath and shows the dramatic change induced by the electric field in the emission bands. Any given optical

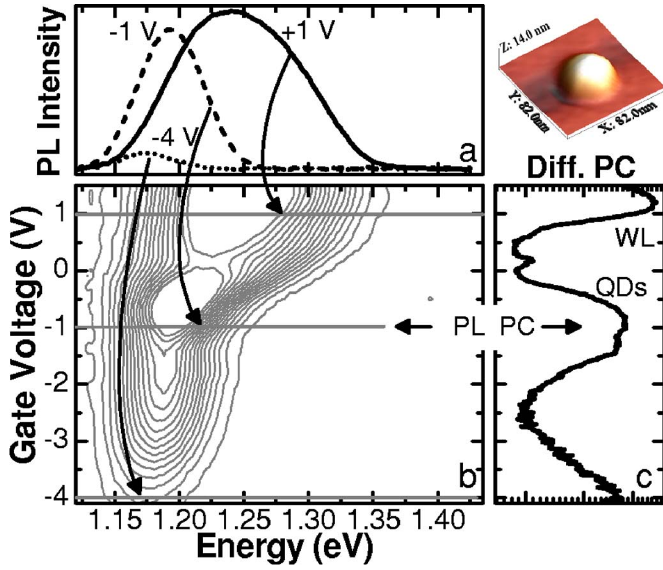

FIG. 3. (Color online) Same as Fig. 1 but for the sample containing quantum dots. Notice the different voltage region covered in this case.

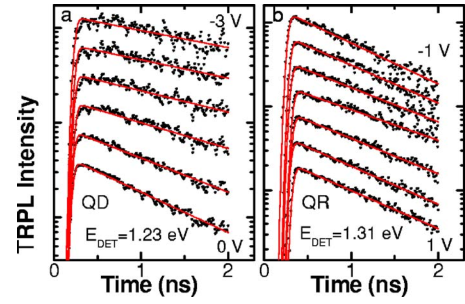

FIG. 4. (Color online) Photoluminescence transient decay curves obtained for quantum dots (left panel) and quantum rings (right panel) varying the external bias. A least squares fit to a single exponential decay function can be used to extract the exciton lifetime at different voltages (solid lines).

transition will be visible only if the electron tunneling rate is smaller (or the same order) than the radiative recombination rate at the applied bias. Due to the energy dependence of both the electronic tunneling rate and the radiative lifetime, the shape of the spectrum changes with the applied voltage, as shown in Figs. 2(b) and 3(b).

Under forward bias, the QR PL spectrum consist of four narrow emission bands at ~1.30, ~1.33, ~1.36, and 1.42 eV, as shown in Fig. 2(a). They correspond respectively to the ground state, first and second excited state, and the wetting layer contributions as discussed previously for Fig. 1(a). Reducing the voltage, the high energy peaks get rapidly quenched, and only the emission from the QR ground state remains visible at −1 V. The large inhomogeneous broadening of the QD sample photoluminescence makes difficult a study of the excited states contribution, but can be exploited to compare the behavior of QDs with different size. As observed in Fig. 3(a), large QDs emitting at ~1.17 eV are still visible at V_g=−4 V, while those emitting around 1.3 eV are already quenched at −1 V as corresponds to their shallower confinement. In this respect, the latter are more similar to QRs and will be further compared with them in the next sections.

Complementary information can be obtained by analyzing the differential PC spectra shown in Figs. 2(c) and 3(c). Under light excitation at 820 nm, we modulate the external voltage at low frequency (177 Hz) and small amplitudes (V_{pp} =10 mV) to obtain the device conductance versus the applied bias using standard lock-in techniques. The differential PC signal is associated with changes in the available density of states $g(E)$ at the Fermi level energy position and in the active region close to the back contact layer.[25,26] At +1 V, both spectra show steep maxima corresponding with the sudden increase of $g(E)$ when the Fermi level crosses the WL continuum. Below this voltage, the signal finds a minimum and rises again when the electrons start tunneling out of the nanostructures. The PL integrated intensity decreases accordingly, as observed in the adjacent panels [Figs. 2(b) and 3(b)]. Two maxima are observed in the QR differential PC spectrum associated with the disappearance of the PL peaks at 1.36 and 1.33 eV, that is, when the Fermi level crosses the electronic excited shells in this sample. Similar resonances, occurring in a more extended region of negative voltages, are also observed in the QD sample, but now they must be associated to carrier tunneling out of increasingly large QDs. Further reverse biasing pins the Fermi level below the fundamental state, and the increase in the differential PC signal indicates the full depletion of photogenerated carriers from the active layer.

Let $n^{E,F}(t)$ be the instantaneous exciton population with energy E when the external bias is F. If we only consider losses associated to radiative recombination and electronic carrier tunneling, we can write for the steady state photoluminescence intensity:

$$I_{PL} \propto \frac{\tau_t^{E,F}}{\tau_r^{E,F} + \tau_t^{E,F}} \quad (1)$$

and it will decrease if either the tunneling time τ_t diminishes, or the radiative time τ_r increases at the given energy and bias. Therefore, continuous wave experiments shown before do not bring any conclusion about which case actually happens. This information can be extracted however, from the TRPL experiments presented in the next sections.

IV. TIME RESOLVED CHARACTERIZATION

Transient decay curves have been recorded in the energy and bias range of interest for both samples. After deconvolution of the system response, the experimental decay curves can be described by single exponential functions revealing the absence of saturation effects [Fig. 4]. This way, we determine the effective exciton lifetime τ as a function of the external voltage for each sample. Quantum dots emitting at 1.23 eV are characterized by a monotonic increase of τ with the reverse bias, as shown in Fig. 4(a). Indeed, the decay time quickly rises from 1.02±0.02 ns at 0 V to 2.65±0.15 ns at V_g=−3 V in this sample. Quantum rings recombining at 1.31 eV show a similar behavior be-

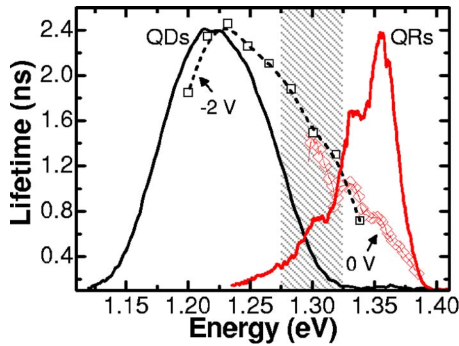

FIG. 5. (Color online) The evolution of τ as a function of the emission energy is shown for QDs (open squares) and QRs (open diamonds). Solid lines represent the PL spectra obtained at +1 V on each sample (T=15 K).

tween 1 V (935±20 ps) and 0 V (1196±30 ps), although τ diminishes back once the device is reverse biased at −1 V (886±30 ps) [Fig. 4(a)]. The region of lifetime increase observed in both samples cannot be explained assuming a constant radiative recombination time independent of the applied electric field. It rather indicates a separation of the electron-hole pair as predicted by the QCSE. Such separation causes a reduction of the exciton oscillator strength that depends on the nanostructure size and shape as discussed below.

In Fig. 5, open squares and open diamonds represent the exciton lifetimes extracted as a function of the PL emission energy for QDs and QRs, respectively. For each sample, the voltage is fixed at the value where τ is close to its maximum. We observe that the exciton lifetime depends strongly on the recombination energy. For the QD sample, τ finds a broad maximum at ~1.23 eV and diminishes slowly at both sides of the emission band. The observation of such maximum could indicate a crossover among two different effects. On the one hand, the radiative recombination time, τ_r, decreases when increasing the exciton coherence volume in large QDs. On the other hand, increasing the dot height at fixed voltage, τ_r must increase due to the enhanced electron-hole pair polarizability induced by the field (see below). The competition of both effects could explain the observed behavior assuming that the exciton coherence volume increases faster than the dot height for these QDs. This assumption seems reasonable for QDs of constant $H/D<1$ ratio and varying height.

The maximum decay time for our QRs occurs at ~0 V. It decreases from ~1.4 ns in the low energy side to less than 300 ps in the high energy tail of the QR emission band, as shown in Fig. 5. Furthermore, the decrease is not monotonous, but stepwise, reflecting the PL band structure. For non-biased systems, such behavior results from the relaxation cascade of photocarriers from the excited states toward the ground state, meaning that the excited states population has a large number of channels open for relaxation and recombination.[27] In our case, in addition to the usual behavior, electrons confined in the excited states are strongly coupled to the adjacent Fermi sea by tunneling. Therefore, in this case, the observed evolution of τ can also be credited to the large barrier penetration of the excited electron wave function.

Figure 5 also allows a direct comparison among QRs and small QDs recombining at nearby energies (shaded region).

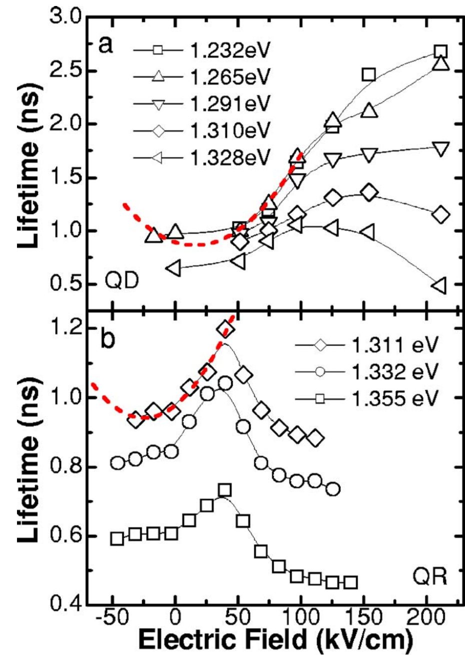

FIG. 6. (Color online) (a) QD sample: The evolution of τ as a function of the electric field is depicted for different recombination energies. The initial region of lifetime increase follows approximately a parabolic dispersion (dashed line). At higher fields the electron tunneling dominates the recombination dynamics diminishing τ. (b) Same as (a) but for the QR sample.

Within the resolution of our experiment, we observe a clear correlation between both curves. Since the electron-hole pair polarizability and the electron tunneling rate determine the maximum value of τ in this energy region, and both magnitudes depend strongly on the height of the nanostructures, at first glance, our result suggests that QRs and QDs emitting at ~1.3 eV have similar vertical confinement profiles. Yet, it should be noted that the maximum lifetime does not occur at the same voltage for both.

The evolution of τ as a function of the external bias at fixed emission energy has been depicted in Fig. 6. The nominal thickness of the intrinsic region d=175 nm provides the electric field strength $F=-(V-V_b)/d$, with V_b=0.7 V deduced from the device capacitance characterization. As discussed above, both samples exhibit a region of monotonous increase of the effective exciton lifetime. As expected, the rate of increase is higher for lower photon energies (larger QDs). Its magnitude ranges from ~14 ps cm/kV for QDs emitting at their peak maximum at 1.23 eV, down to ~5 ps cm/kV for QDs emitting at 1.31 eV [Fig. 6(a)]. In the next section, this behavior will be analyzed considering a simplified confinement potential for our QDs. Now, the differences found among QDs and QRs should be noted. The QR's ground state exciton lifetime is more rapidly affected by the field, being abruptly modified in a shorter bias range [Fig. 6(b), diamonds]. Since the exciton polarization properties strongly depends on the size, shape, and composition of these nanostructures, the differences should be related to their particular confining potential.[28,29] Even in the absence of an electric field, due to the different effective masses and

strain dependence of the valence and conduction band edges, the electron and the hole center of masses are spatially separated along the growth direction.[28,30,31] When the electron lies above the hole, a negative dipole moment is created, being its direction opposite to the field for $F>0$. In such a situation, there will be a maximum of the electron-hole overlap when the field action cancels the initial carrier separation at some positive value of the field. It follows that, both, the emission rate, and the exciton recombination energy, will reach a maximum at this critical field. This is the expected situation for a pure InAs QD whose lateral dimensions diminish from the base to the apex.[28] To find the opposite alignment, the hole above the electron, a certain Ga-In alloying is necessary, with the indium composition increasing from the base to the top of the tapered nanostructure.[28] The maximum electron-hole overlap occurs then at $F<0$. Figures 6(a) and 6(b) include two parabolic fits roughly describing the quadratic dispersion predicted by the QCSE in the bias region where the tunneling is still negligible.[32,31] According to these fits, the minimum of the radiative lifetime takes place at ~ -25 kV/cm for QRs in their ground state, and at ~ 16 kV/cm for QDs near to the center of their inhomogeneous emission band. This result suggests, within the limited validity of the perturbation theory applied to this case,[29] that both kinds of nanostructures exhibit permanent dipole moments with opposite signs. In particular, our result implies a constant composition profile for these QDs, and the presence of a noticeable In-Ga composition grading introduced during the annealing step that gives rise to these QRs.[21,33]

V. ADIABATIC CALCULATION OF THE RADIATIVE AND TUNNELING RATES

In the following, the bias evolution of the exciton lifetime is estimated for QDs with different sizes and simplified geometry. The model reproduces the behavior observed by increasing the vertical confinement in the QD providing a fair agreement with the experimental values shown in Fig. 6(a). Given the rather flat aspect ratio of these QDs, at zero field, the wave function spreads mainly in the lateral plane, whereas, in the presence of the field, the magnitude of the QCSE depends mainly on the vertical confinement potential. Therefore, we solve adiabatically the effective mass Schrödinger equation for a single electron-hole pair confined by a lateral parabolic potential and a vertical square potential in the presence of an external electric field. In the strong confinement regime, the electron-hole pair wave function is described by the electron and hole single particle envelope wave functions:

$$\Psi_{eh}(\rho_e,\rho_h,z_e,z_h) = s_e(\rho_e)s_h(\rho_h)f_e(z_e)f_h(z_h). \qquad (2)$$

We use a complex Airy function numerical method to solve the field-dependent vertical confinement potential and obtain the wave functions f_i.[34,35] The band offsets are calculated assuming a biaxially strained InAs/GaAs QW with the deformation potentials, elastic constants, and band profiles listed by Stier *et al.*[30] We consider a single dielectric constant along the heterostructure but we take into account different effective masses at the dot boundaries. Next, the two-dimensional harmonic potential ground state wave functions, s_i, are parametrized by the carrier confinement length $l_i = \sqrt{\frac{\hbar}{m_i^* \omega_i}}$, where m_i^* is the carrier effective mass and $\hbar\omega_i$ is its in-plane confinement energy.[36] With these definitions, the oscillator strength for our optical transition can be readily calculated using (Ref. 37):

$$f = \frac{E_p}{2E}\left|\int \Psi_{eh}(\rho_e,\rho_h,z_e,z_h)\,\delta(\vec{r_e}-\vec{r_h})dV\right|^2, \qquad (3)$$

where E_p and E are the Kane energy and the transition energy, respectively. The overlap integral determines the maximum oscillator strength attainable. For perfect overlap among the electron and the hole, the oscillator strength yields $f\sim 10.4$ for a QD emitting at 1.23 eV with $E_p(\text{GaAs})=25.7$ eV. This is a value typically found in both ensemble and single QD absorption experiments.[13,38] The corresponding exciton radiative lifetime is given by (Ref. 13):

$$\tau_r = \frac{6\pi\epsilon_0 m_0 c^3\hbar^2}{e^2 n f E^2} \qquad (4)$$

and yields $\tau\sim 1.2$ ns when $n(\text{GaAs})=3.59$. This value is close to the experimental values found for both QRs and QDs in their fundamental state at 0 V [Figs. 5(a) and 6(a)], but, it should be noted that the perfect overlap assumed here is not the general case even at zero field. For the neutral ground exciton, holes are confined laterally more strongly than electrons with typical confinement length ratios $a = l_e/l_h \sim 1.5-3$. [23,38,39] In the lateral parabolic potential used here, these values translate into an in-plane overlap integral $|\langle s_e|s_h\rangle| = \frac{2a}{1+a^2}$ between 0.92 and 0.6, imposing an upper limit for the maximum achievable oscillator strength within the model.[36]

This said, the evolution of the oscillator strength with the electric field depends solely on the vertical confinement potential. Introducing the factor $C(E)$ derived from the precedent expressions, the field-dependent emission rate, $\tau_r^{-1} = C(E)|\langle f_e|f_h\rangle|^2$, can be calculated. Similarly, the electron tunneling rate, τ_t^{-1}, can be extracted directly from the complex Airy function method.[34,35] To do so, first, the addition energies for the vertical confining potential $E_e(F)$ are calculated. Next, to account for the lateral confinement potential, these energies are rigidly shifted, being $E_e = E_e(F) + \hbar\omega_e$ the total electron energy relevant for the tunneling time calculation. Alternately, τ_t^{-1} has been also estimated evaluating the Wentzel-Kramers-Brillouin approximated expression at the same energy (Ref. 40):

$$\frac{1}{\tau_t} = \frac{\hbar}{8m_e^* H^2}\exp\left[-\frac{4}{3}\frac{\sqrt{2m_e^*}}{e\hbar F}(\Delta E_c - E_e)^{3/2}\right]. \qquad (5)$$

Thick solid lines in Fig. 7 show the result of this theoretical scheme. A constant ratio $H/D=1/3$ has been assumed, with $D=2l_e=2l_h$ determining both the lateral potential confinement energies, ω_i, and the in-plane overlap integral. As expected, the effective exciton lifetime increases when $F>0$ reaching a maximum and diminishing later. For the chosen band offsets ($\Delta E_c=607.5$ meV, $\Delta E_v=376.6$ meV),

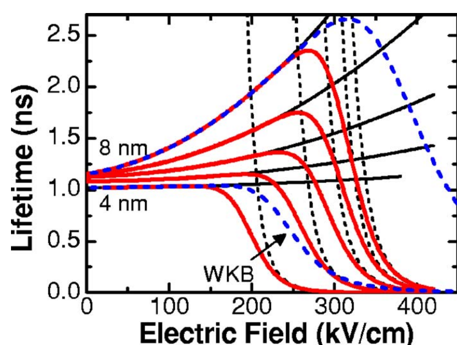

FIG. 7. (Color online) Thick solid lines represent the effective lifetime obtained for different QD heights following the adiabatic model discussed in the text. A constant aspect ratio $H/D=1/3$ has been assumed in all cases. The elementary radiative and tunneling contributions are represented by solid and dashed thin lines, respectively. Thick dashed lines are obtained evaluating the WKB formula at the same electron energies [Eq. (5)].

4-nm thick QDs are weakly affected by the field before reaching the tunneling regime. Increasing the dot height (H) from 4 to 8 nm, the maximum radiative lifetime attainable increases from ~1 ns to ~2.5 ns reproducing quite well the experimental values found for the inhomogeneously broadened QD emission band [Fig. 6(a)].

Despite the general agreement, we note that the maximum values are reached at lower electric fields in the experiment than in the model. In other words, our calculation underestimates the QD polarizability, being especially true for the smaller QDs where the models do not predict any lifetime increase at all. Our experimental results rather suggest that excitons confined in QRs and small QDs can be significantly polarized by the electric field. The model can describe successfully the contribution of the QCSE to the recombination dynamics in large QDs giving an overall good agreement with the experiment. More accurate theoretical predictions can only be provided if the real shape, size, and composition profiles derived from available structural information are introduced.[33] The discrepancies found for the small QDs and the QRs must be attributed therefore to the approximations made in our simplified adiabatic scheme.

VI. CONCLUSIONS

We have investigated the role played by the QCSE in self-assembled nanostructures with different size and shape focusing on their recombination dynamics. We systematically find an increase of the exciton radiative lifetime at moderate electric fields. While the absolute magnitude of this effect depends on the nanostructure size, this main conclusion remains valid in the whole energy range studied here. Given the large interest in the coherent manipulation of single quantum states, we believe that the reduction of the oscillator strength reported here must be considered in future developments.

ACKNOWLEDGMENTS

The authors gratefully acknowledge financial support by the Spanish MEC and CAM through Projects Nos. TEC-2005-05781-C03-01/03, NAN2004-09109-C04-01/03, CSD2006-0019, and S-505/ESP/000200, and by the European Commission through the SANDIE Network of Excellence (Contract No. NMP4-CT-2004-500101).

*Electronic address: benito@imm.cnm.csic.es

[1] E. E. Mendez, G. Bastard, L. L. Chang, L. Esaki, H. Morkoc, and R. Fischer, Phys. Rev. B **26**, 7101 (1982).
[2] D. A. B. Miller, D. S. Chemla, T. C. Damen, A. C. Gossard, W. Wiegmann, T. H. Wood, and C. A. Burrus, Phys. Rev. Lett. **53**, 2173 (1984).
[3] G. Bastard, E. E. Mendez, L. L. Chang, and L. Esaki, Phys. Rev. B **28**, 3241 (1983).
[4] K. Köhler, H. J. Polland, L. Schultheis, and C. W. Tu, Phys. Rev. B **38**, 5496 (1988).
[5] D. Haft, R. J. Warburton, K. Karrai, S. Huant, G. Medeiros-Ribeiro, J. M. García, W. Schoenfeld, and P. M. Petroff, Appl. Phys. Lett. **78**, 2946 (2001).
[6] K. Kowalik, O. Krebs, A. Lemaitre, S. Laurent, P. Senellart, P. Voisin, and J. A. Gaj, Appl. Phys. Lett. **86**, 041907 (2005).
[7] S. Seidl, M. Kroner, A. Högele, K. Karrai, R. J. Warburton, A. Badolato, and P. M. Petroff, Appl. Phys. Lett. **88**, 203113 (2006).
[8] F. Findeis, M. Baier, E. Beham, A. Zrenner, and G. Arbsreiter, Appl. Phys. Lett. **78**, 2958 (2001).
[9] R. Oulton, J. J. Finley, A. D. Ashmore, I. S. Gregory, D. J. Mowbray, M. S. Skolnick, M. J. Steer, S.-L. Liew, M. A. Migliorato, and A. J. Cullis, Phys. Rev. B **66**, 045313 (2002).
[10] R. Oulton, A. I. Tartakovskii, A. Ebbens, J. Cahill, J. J. Finley, D. J. Mowbray, M. S. Skolnick, and M. Hopkinson, Phys. Rev. B **69**, 155323 (2004).
[11] S. Seidl, M. Kroner, P. A. Dalgarno, A. Högele, J. M. Smith, M. Ediger, B. D. Gerardot, J. M. García, P. M. Petroff, K. Karrai *et al.*, Phys. Rev. B **72**, 195339 (2005).
[12] M. Bayer and A. Forchel, Phys. Rev. B **65**, 041308(R) (2002).
[13] B. Alén, F. Bickel, K. Karrai, R. J. Warburton, and P. M. Petroff, Appl. Phys. Lett. **83**, 2235 (2003).
[14] A. Högele, B. Alén, F. Bickel, R. J. Warburton, P. M. Petroff, and K. Karrai, Physica E (Amsterdam) **21**, 175 (2004).
[15] F. Yang, K. Hinzer, C. N. Allen, S. Fafard, G. C. Aers, Y. Feng, J. McCaffrey, and S. Charbonneau, Superlattices Microstruct. **25**, 419 (1999).
[16] R. M. Thompson, R. M. Stevenson, A. J. Shields, I. Farrer, C. J. Lobo, D. A. Ritchie, M. L. Leadbeater, and M. Pepper, Phys. Rev. B **64**, 201302(R) (2001).
[17] J. M. Smith, P. A. Dalgarno, R. J. Warburton, A. O. Govorov, K. Karrai, B. D. Gerardot, and P. M. Petroff, Phys. Rev. Lett. **94**, 197402 (2005).
[18] A. S. Dissanayake, J. Y. Lin, and H. X. Jiang, Phys. Rev. B **51**, 5457 (1995).
[19] G. W. Wen, J. Y. Lin, H. X. Jiang, and Z. Chen, Phys. Rev. B **52**,

5913 (1995).
[20] J. Müller, J. M. Lupton, P. G. Lagoudakis, F. Schindler, R. Koeppe, A. L. Rogach, and J. Feldmann, Nano Lett. **5**, 2044 (2005).
[21] D. Granados and J. M. García, Appl. Phys. Lett. **82**, 2401 (2003).
[22] J. M. García, D. Granados, J. P. Silveira, and F. Briones, Microelectron. J. **35**, 7 (2004).
[23] B. Alén, J. Martínez-Pastor, D. Granados, and J. M. García, Phys. Rev. B **72**, 155331 (2005).
[24] C. Rudamas, J. Martínez-Pastor, A. García-Cristóbal, P. Roussignol, J. M. García, and L. González, Phys. Status Solidi A **190**, 583 (2002).
[25] G. Medeiros-Ribeiro, J. M. García, and P. M. Petroff, Phys. Rev. B **56**, 3609 (1997).
[26] D. V. Lang, J. D. Cohen, and J. P. Harbison, Phys. Rev. B **25**, 5285 (1982).
[27] F. Adler, M. Geiger, A. Bauknecht, F. Scholz, H. Schweizer, M. H. Pilkuhn, B. Ohnesorge, and A. Forchel, J. Appl. Phys. **80**, 4019 (1996).
[28] J. A. Barker and E. P. O'Reilly, Phys. Rev. B **61**, 13840 (2000).
[29] W. Sheng and J. P. Leburton, Phys. Rev. B **67**, 125308 (2003).
[30] O. Stier, M. Grundmann, and D. Bimberg, Phys. Rev. B **59**, 5688 (1999).
[31] J. A. Barker, R. J. Warburton, and E. P. O'Reilly, Phys. Rev. B **69**, 035327 (2004).
[32] P. Fry, I. E. Itskevich, D. J. Mowbray, M. S. Skolnick, J. J. Finley, J. A. Barker, E. P. O'Reilly, L. R. Wilson, I. A. Larkin, P. A. Maksym *et al.*, Phys. Rev. Lett. **84**, 733 (2000).
[33] P. Offermans, P. M. Koenraad, J. H. Wolter, D. Granados, J. M. García, V. M. Fomin, V. N. Gladilin, and J. T. Devreese, Appl. Phys. Lett. **87**, 131902 (2005).
[34] R. Enderlein, T. Holz, and J. L. Gondar, Phys. Status Solidi B **156**, 259 (1989).
[35] S. Panda and B. K. Panda, Pramana **56**, 809 (2001).
[36] R. J. Warburton, B. T. Miller, C. S. Dürr, C. Bödefeld, K. Karrai, J. P. Kotthaus, G. Medeiros-Ribeiro, P. M. Petroff, and S. Huant, Phys. Rev. B **58**, 16221 (1998).
[37] J. H. Davies, *The Physics of Low-Dimensional Semiconductors: An Introduction* (Cambridge University Press, London, 1996).
[38] R. J. Warburton, C. S. Dürr, K. Karrai, J. P. Kotthaus, G. Medeiros-Ribeiro, and P. M. Petroff, Phys. Rev. Lett. **79**, 5282 (1997).
[39] J. J. Finley, P. W. Fry, A. D. Ashmore, A. Lemaitre, A. I. Tartakovskii, R. Oulton, D. J. Mowbray, M. S. Skolnick, M. Hopkinson, P. D. Buckle *et al.*, Phys. Rev. B **63**, 161305(R) (2001).
[40] W. Heller, U. Bockelmann, and G. Abstreiter, Phys. Rev. B **57**, 6270 (1998).